

Stain-Refinement and Boundary-Enhancement Weight Maps for Multi-organ Nuclei Segmentation

Ruochan Wang

*Graduate School of Information, Productions and System
Waseda University
Kitakyushu, Japan
ayaka_ou@akane.waseda.jp*

Sei-ichiro Kamata

*Graduate School of Information, Productions and System
Waseda University
Kitakyushu, Japan
kam@waseda.jp*

Abstract—Nuclear detection and segmentation in pathological images is a crucial prerequisite for finding and forecast of numerous ailments. With the advancement of deep learning, high precision automatic segmentation of multi-organ nuclei pathological images is possible. The segmentation results require not only accurate foreground prediction but also careful annotation of every individual object. There are still several remaining challenges in multi-organ nuclei segmentation. Firstly, blurred boundaries and inconsistent staining make pixel-wise segmentation difficult to generate occlusive object masks. Secondly, the background noise will be retained or even enhanced after preprocessing. Thirdly, the differences in size, shape, and intensity of different organs make it harder to separate touching nuclei. Two novel weight maps of loss function are proposed, which make full use of structural information provided by raw image and its corresponding annotations, in order to supervise the network learning more available features. The Stain Refinement Weight Map focuses on the structural difference between Hematoxylin channel and Eosin channel, which has been neglected in existing methods, to highlight potential noise pixels. The Boundary-Enhancement Weight Map leverages the new boundary annotation of each individual object that has emerged in the recent dataset to help the network better divide cell clusters. We test our method on Multi-Organ Nuclei Segmentation Dataset and show that our proposed method has high accuracy in nuclei detection and can separate touching nuclei effectively in the segmentation task.

Contribution—The main contribution of this paper is to propose two pre-defined novel weight maps to help the network extract better features.

Index Terms—H&E image, Nuclei Segmentation, Deep Learning, Semantic Segmentation, Pixel-wise Weight Map

I. INTRODUCTION

Automatic analysis of digital pathological images is one demanding research topic recently. Segmentation of nuclei from cell images is helpful for pathological diagnosis and prognosis since the size, shape, and intensity of a single cell nucleus and the density of nuclei in the region are all important indicators of the cancer grading system. A cytopathic image may contain thousands of nuclei. Analyzing the pathological images manually takes a lot of time, and subjective judgments from different experts for the same picture will be very different. Hence, automatic pathological image analysis with high accuracy is required.

H&E image is the most widely used cytopathological image type. Different dyes will bind to different cellular structures. As shown in Fig. 1(a), The nucleus is stained into purple under

the effect of Hematoxylin, and Eosin stains the cytoplasm pink. In order to better separate the nucleus from other structures, some preprocessing methods are required. The traditional preprocessing method only selects one channel from RGB channels as the input image, but this method cannot distinguish the nucleus and cytoplasm well. Color Deconvolution is proposed for separating different components [1]. The cellular RGB image is converted into optical density image. With the empirically known color appearance matrix, the stain density matrix is extracted, which preserves structure information of the individual cellular components. The H channel image and E channel image can be extracted by color deconvolution, which respectively represents the structure pictures stained by Hematoxylin and Eosin in the original picture. SNMF method is an improvement on the traditional color deconvolution approach, which utilizes sparse non-negative matrix factorization to factor out a specific color appearance matrix for each picture, instead of a fixed and common used color appearance matrix [2]. Most current nuclei segmentation methods use H channel images extracted by SNMF as the input images.

With the development of deep learning, it is possible to segment multi-organ nuclei with high accuracy. Fig. 2 shows that nuclei of different organs have a significant difference in shape, size, and intensity. Unsupervised methods such as [3], [4] are difficult to extract single feature type to segment nuclei from different organs. In contrast, deep learning methods can automatically learn features from the given task. However, several challenges still remain. Firstly, the previously mentioned color separation method is to infer its structure based on color information in the images, which means some noise caused by the staining process and background pollution will still be retained. These noises have a high probability of being judged as nuclei. Secondly, the existence of cell clusters makes the accurate segmentation of individual cells difficult. Thirdly, blurred boundaries and inconsistent staining makes pixel-wise segmentation prone to loss of spatial information, such as predicting a hole in the nucleus.

SAMS-Net [5] compares H channel pixel intensity with ground truth and constructs weight maps to make the segmentation network sensitive to the change of hematoxylin intensity. In order to enable the network to obtain the features of an individual nucleus and its edge, morphological operations and

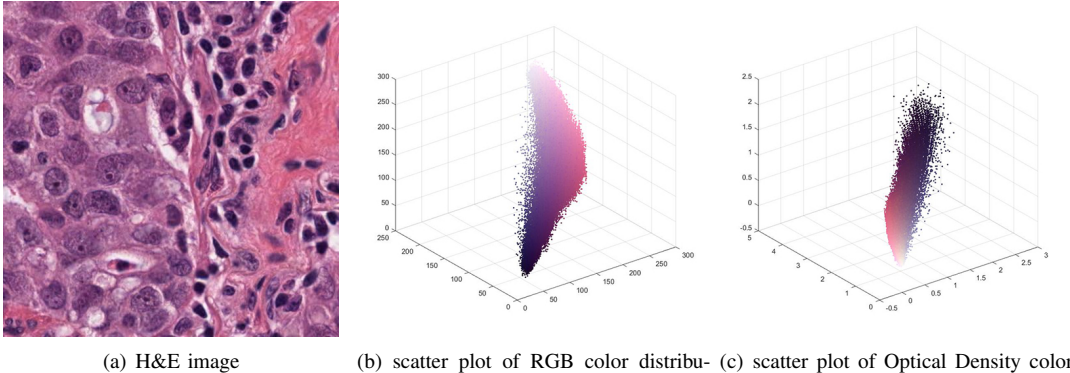


Fig. 1. Color distribution of H&E image

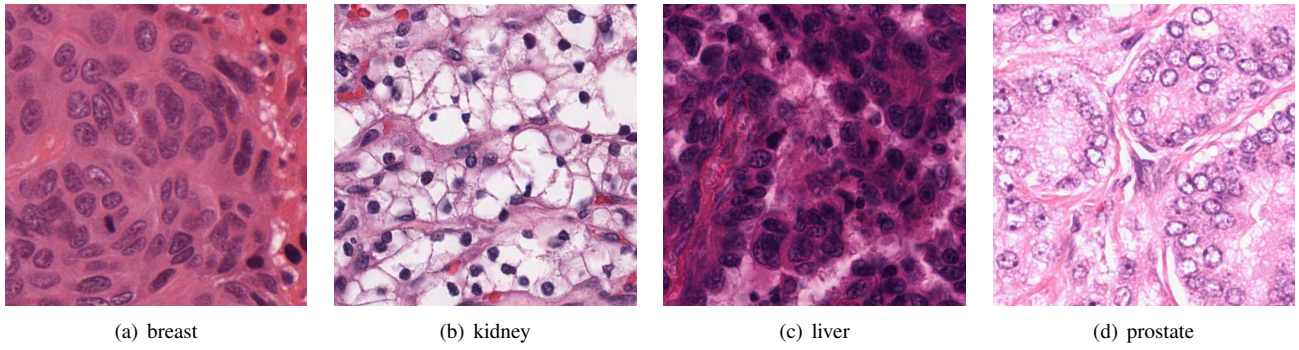


Fig. 2. tissue images of different organs

artificial 1-pixel-wide background are commonly used, such as [6], [7]. Concave features of cell clusters were used to divide overlapping nuclei. The Multi-organ nuclei dataset [8] makes it possible to learn the exact morphological characteristics of every single nucleus. CIA-Net [9] proposed Information Aggregation Module to achieve the bi-directionally feature aggregation to improve the decoder part of the network. The group-equivariant layers [10] are also used to replace the traditional convolution layer of U-Net to make the network rotation invariance. Conditional GAN [11] is used to enhance the spatial correlation of segmentation results.

Most of the above methods only use H channel images in the network. We have mentioned this still introduces noise, and discarding E channel images means to lose some structural information. To reduce the negative impact of noise in H channel, we introduce a novel Stain Refinement Weight Map to give higher weight to the boundary pixels and potential noise pixels by calculating the likelihood between H channel and E channel image.

Existing segmentation methods [9]–[11] for multi-organ nuclei images all focus on the modifying of deep learning network structure but fail to make use of the potential rich edge information in the given dataset. Our Boundary Enhancement Weight Map utilizes the edge information of given ground truth to help the touching area separated better.

This paper mainly contributes to two pre-defined novel weight maps that focus on the similarity between nuclei

components and precise boundaries on touching nuclei, respectively.

The remainder of this paper follows the following structure. Section II describes the proposed approach in detail. Section III shows the experiment results. Finally, our work is concluded in Section IV.

II. PROPOSED METHOD

A. Color Separation

Stain separation methods estimate how the different stains behave in RGB space and estimate the stain density of different components. By Beer-Lambert Law, an RGB image can be translated to an Optical Density image. Fig. 1(b) and 1(c) show that color distribution in RGB space is nonlinear, but in Optical Density space is linear. $I \in \mathbb{R}^{m \times n}$ is the matrix of RGB intensity, here $m = 3$ represents the channel number of RGB space, and n is the total number of image pixels. I_0 is the incident light intensity that passing through the slide. For 8 bit images, I_0 is usually 255 or the max pixel intensity in the image. I and I_0 have the relationship as follows [12]:

$$I = I_0 \cdot \exp(-BX) \quad (1)$$

Here $B \in \mathbb{R}^{m \times r}$ is color appearance matrix. The columns show how different stain behave in RGB space. $X \in \mathbb{R}^{r \times n}$ is the stain density map that each row represents the concentration of every staining reagent. Here r is the number of reagent types, in H&E image, $r = 2$.

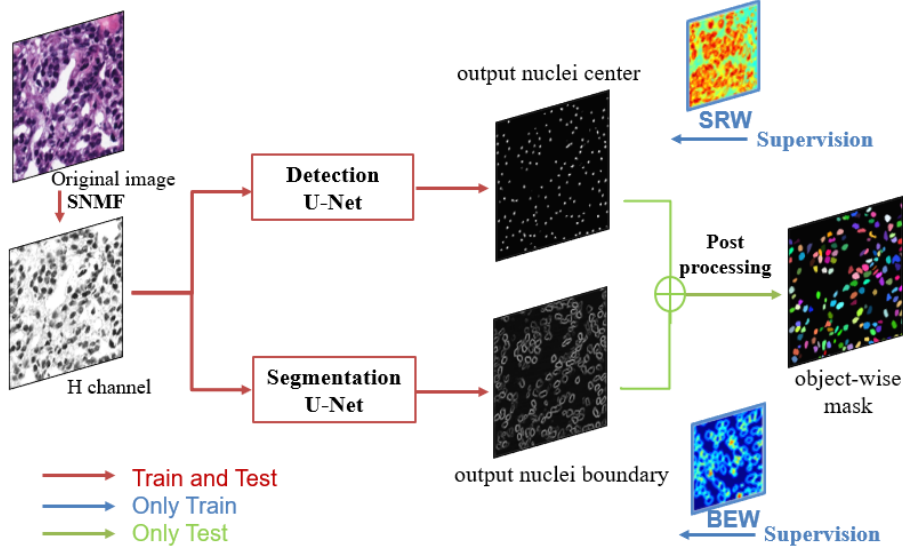


Fig. 3. Overall framework of proposed method.

We can also calculate Optical Density image V from RGB image I :

$$V = \log \frac{I_0}{I} \quad (2)$$

Therefore:

$$V = BX \quad (3)$$

Here, V can be got from observation, and by decomposition of V , we can get color appearance matrix B as well as stain density matrix X . SNMF [2] is now the most commonly used method of decomposition. After SNMF method to get B and X , we can obtain intensity image of Hematoxylin stained component as H_{OD} and Eosin stained component as E_{OD} .

$$H_{OD} = B(:, 1) \times X(1, :) \quad (4)$$

$$E_{OD} = B(:, 2) \times X(2, :) \quad (5)$$

H channel image I_h and E channel image I_e in RGB space can be then reconstructed from H_{OD} and E_{OD} .

B. Loss Function of U-Net

Fig. 3 reveals the overall framework of our approach. H channel image is extracted as the input of the network. Here we use U-Net [13] for nuclei detection and boundary segmentation.

For different tasks, two different weight maps are used for supervision. After detecting the center of each nucleus and extracting all boundaries pixels, we assign boundaries for every nucleus center.

U-Net is an encoder-decoder network with skip connections to achieve end-to-end semantic segmentation. It is widely used in medical images since its excellent performance on small datasets. For 2-class segmentation, the pixel-weighted

soft-max cross-entropy loss for U-Net can be written like following:

$$\mathcal{L} = - \sum_{x \in \Omega} w(x) \cdot \log \frac{\exp(\hat{y}_{y(x)}(x))}{\exp(\hat{y}_1(x)) + \exp(\hat{y}_0(x))} \quad (6)$$

Here x is one of the pixels in the image Ω , $\hat{y}_1(x)$ represents the predicted probability about x is a foreground pixel, $\hat{y}_0(x)$ is the predicted probability about x is a background pixel, $\hat{y}_{y(x)}(x)$ is the predicted probability when x belongs to its ground truth label $y(x)$, $y(x) = 1$ or 0 . w is the pixel-wise loss weight map.

C. Stain Refinement Weight Map

Based on (6), we propose a Stain Refinement Weight Map w_{SRW} to give higher weights to pixels which will be easily misjudged.

For every single H&E image I in RGB space, H channel image I_h and E channel image I_e can be separated. It is important to note that this color separation process is nonlinear in RGB space. Usually, the H channel image I_h is used as the input image of the network, and E channel image I_e is neglected. This will cause loss of structural information. In stain density map X , every column represents how Hematoxylin and Eosin impact the pixel. If the values of the two elements are similar, that means this pixel may be stained by two dyes at the same time and will be hard to separate. Therefore, for Hematoxylin image I_h and Eosin image I_e of the same original image I , we propose a Stain Refinement Weight Map w_{SRW} to estimate the similarity between I_h and I_e :

$$w_{SRW} = \exp(-|I_h - I_e|), \quad (7)$$

Fig. 4 shows the H channel image and E channel image from the same original H&E image. For nuclei detection and segmentation, nuclei pixels (foreground pixels) need to

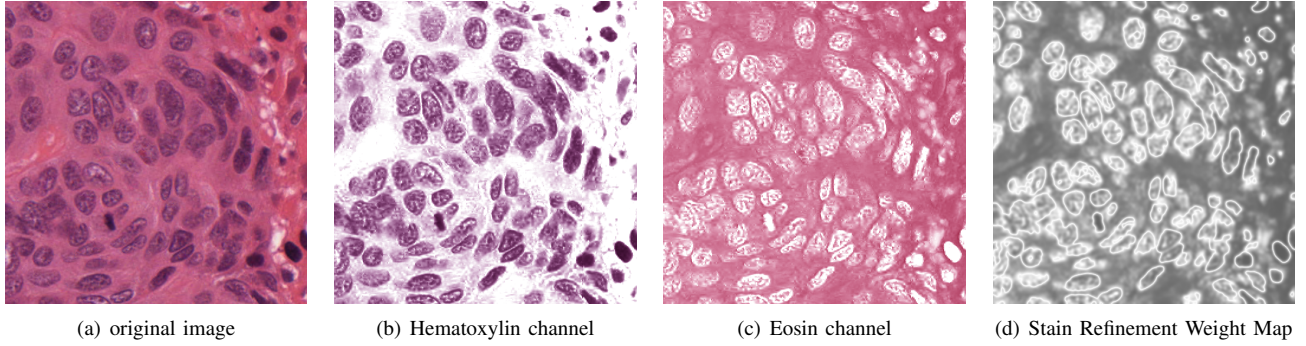


Fig. 4. Structure Comparison of Hematoxylin channel image and Eosin channel image

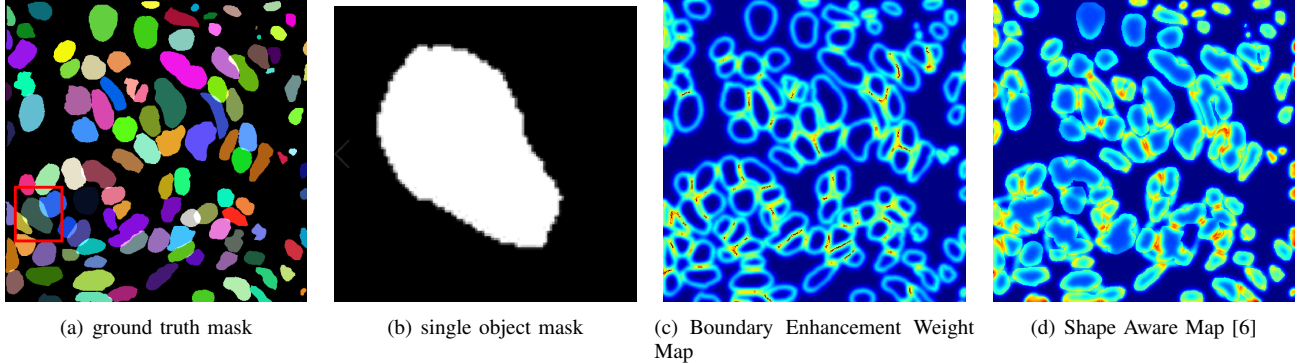


Fig. 5. Generated Boundary Enhancement Weight Map from careful annotations of individual object mask

have low intensity, in other words, need to be dark, while the background pixels need to be bright. It is observable that Stain Refinement Weight Map can highlight not only the background pixels that have low intensity, but also the foreground pixels that have high intensity and boundary pixels. All these three situations may cause misclassification while segmenting because of the abnormal staining.

D. Boundary Enhancement Weight Map

To help the network separate touching objects, we propose a Boundary Enhancement Weight Map w_{BEW} to give higher weight to pixels of nuclei boundary and pixels near the boundary, especially in touching regions. Unlike other public datasets previously provided, As shown in Fig. 5(a), 5(b), MoNuSeg dataset not only provides binary ground truth mask of foreground pixels but also give boundary annotation of every single nucleus. To take the full advantages of given data, the Boundary Enhancement Weight Map w_{BEW} is designed as follows:

$$w_{BEW} = \Phi_F + (F_\sigma * G) \times \Phi_B \quad (8)$$

Here G is boundary ground truth mask, F_σ is a gaussian filter which can propagate values from boundary pixels to its neighboring pixels [6]. Φ_F and Φ_B are the distance transformation of foreground pixels and background pixels respectively:

$$\Phi_F = \exp\left(-\frac{d(x)^2}{2\sigma_F^2}\right) \quad (9)$$

$$\Phi_B = \exp\left(-\frac{(d_1(x) + d_2(x))^2}{2\sigma_B^2}\right) \quad (10)$$

For boundary pixel x of one object, $d(x)$ is the distance from x to the nearest boundary pixel of other objects. For pixel x which is not the boundary, $d_1(x)$ and $d_2(x)$ is the distance from pixel x to the nearest and second nearest boundary pixel.

Fig. 5(c) and 5(d) shows our proposed Boundary Enhancement Weight Map w_{BEW} and Shape Aware Map (SAW) proposed by Fidel et al. [6], respectively. SAW was generated by the outer edge of nuclei clusters. Comparing these two weight maps, our proposed method can help the network learning more accurate touching region information.

The foreground pixels are usually less than background pixels, which means it may be hard to learning foreground features because of the lack of pixel amounts. Therefore, the Class Balance Weight w_c is used:

$$fw = \frac{1}{foreground\ pixel\ amount} \quad (11)$$

$$bw = \frac{1}{background\ pixel\ amount} \quad (12)$$

$$fw_{norm} = \frac{fw}{max(fw, bw)} \quad (13)$$

$$bw_{norm} = \frac{bw}{max(fw, bw)} \quad (14)$$

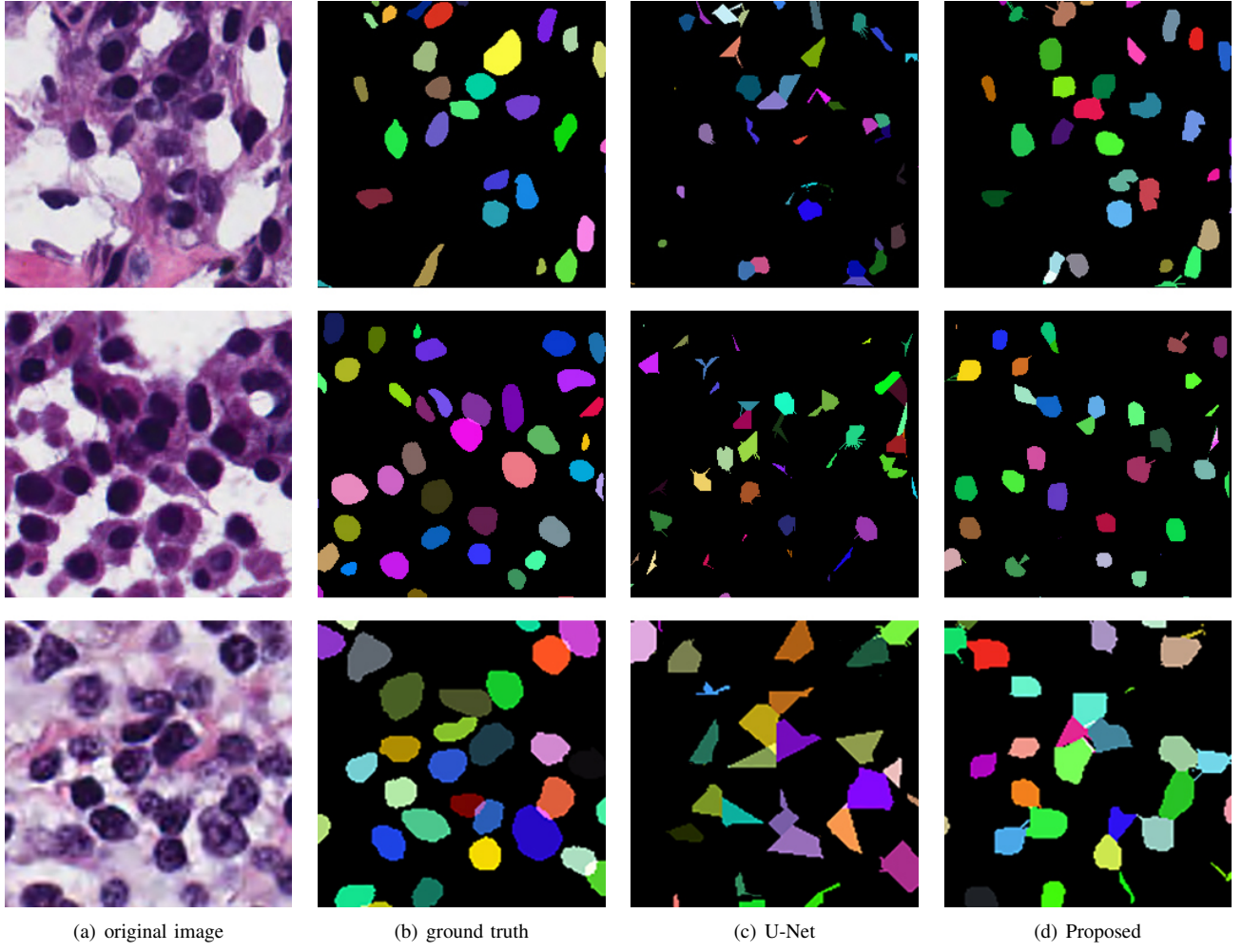


Fig. 6. Experiment Results

$$w_c(x) = \begin{cases} fw_{norm} & x \in foreground \\ bw_{norm} & x \in background \end{cases} \quad (15)$$

The overall weight maps w_D for nuclei detection and w_S for nuclei boundary segmentation is used for network training:

$$w_D = w_c + w_{SRW} + 1 \quad (16)$$

$$w_S = w_c + w_{BEW} + 1 \quad (17)$$

III. EXPERIMENT RESULTS

A. Dataset

MoNuSeg dataset [8] of 2018 MICCAI challenge provide complete pixel-level annotations of H&E image. There are 30 training images with the size of 1000×1000 . The training images contain around 22000 nuclei from 7 diverse organs (breast, kidney, prostate, liver, colon, bladder, and stomach). Another 14 test images provide additional 7000 nuclei boundary annotations with 7 organs (kidney, prostate, lung, bladder, breast, colon, and brain). Two organs in the testing dataset didn't appear in the training dataset. All of these training and testing images were extracted from TCGA archive. These

images come from different patients, different hospitals with different staining protocols. Both benign and malignant cases exist.

B. Preprocessing and Implementation

Our proposed method is validated on MoNuSeg dataset, using all of the 30 training images and 14 testing images. The mentioned SNMF color unmixing method is utilized to extract the Hematoxylin channel grayscale images as the input images of U-Net. To avoid excessive computational complexity but still ensure accurate prediction accuracy at the same time, the input images are cropped into 256×256 patches for training and testing.

We carried out several experiments to observe the effects of different initial learning rates on the two tasks, respectively. Too high initial learning rate will lead to non-convergence of the loss function. Also, the predicted probability map is rather fuzzy. In contrast, the low initial learning rate is difficult for convergence. The predicted result is a kind of over-fitting. Finally the model was trained for 200 epochs. An initial learning rate of 10^{-4} is utilized for nuclei detection, and 10^{-5} is utilized for boundary segmentation.

C. Evaluation Metrics

After the assignment, for every detected nuclei center, we assign boundary pixels to it. For nuclei detection, on condition that the predicted center and ground truth have the distance less than 6 pixels, it is regarded as true positive. $F1 - score = \frac{2 \cdot precision \cdot recall}{precision + recall}$ is used to evaluate the detection results.

For nuclei segmentation, we have the ground truth labels set $G = \{G_1, G_2, \dots, G_m\}$ and predicted masks set $P = \{P_1, P_2, \dots, P_n\}$. For every ground truth object G_i , find the relative predicted P_j which $j = \operatorname{argmax}_k \frac{G_i \cap P_k}{G_i \cup P_k}$. N is the set that predicted objects have no intersection with ground truth. Average Jaccard Index (AJI) and $F1$ score are used for evaluation.

$$AJI = \frac{\sum_{i=1}^n G_i \cap P_j}{\sum_{i=1}^n G_i \cup P_j + \sum_{k \in N} P_k}, \quad (18)$$

We compare our detection result with the unsupervised method [14] and traditional U-Net [13] without the weight map. Table I show the *precision*, *recall*, and $F1 - score$ of different methods.

Unsupervised methods usually focus on the morphological characteristics of single type organ nuclei, so they cannot be applied to the segmentation of multi-organ nuclei. However, due to the nuclear pixels have small proportion in the whole slide image, moreover, the background containing noise, class imbalance, and noise make traditional U-Net easy to over detect. The detection result has a high recall, but the precision is low. Compared with the above methods, our proposed method can adapt to different sizes and shapes of nuclei, and strike a balance between precision and recall.

TABLE I
COMPARISON OF DIFFERENT METHODS ON NUCLEI DETECTION

method	precision	recall	$F1$ score
gLoG [14]	0.2988	0.7115	0.4208
U-Net [13]	0.4812	0.8566	0.6162
Proposed	0.8215	0.8404	0.8308

Fig. 6 shows the comparison of segmentation result between standard U-Net and U-Net with our proposed weight maps. Because we just segment boundary pixels, the foreground has very few pixel amount, traditional U-Net without class balance and boundary enhancement could not learn boundary features very well. Some of the detected boundaries are not occlusive, hence after postprocessing, the generated masks are not smooth and loss many foreground areas.

Comparing to ground truth labels, the proposed approach can separate touching nuclei well. Also, for some noise regions which may cause mislabeling, our method can segment these regions correctly. Table II shows the quantitative evaluation result compared with traditional U-Net [13] and Enhanced U-Net [10]. Tab III shows the evaluation for each organ compared with traditional U-Net.

IV. CONCLUSION

We propose two weight maps for nuclei detection and boundary segmentation. The Stain Refinement Weight Map

TABLE II
QUANTITATIVE EVALUATION RESULT COMPARISON

method	$F1$ score	AJI
U-Net [13]	0.5979	0.4568
Enhanced U-Net [10]	0.8469	0.6291
Proposed	0.8222	0.6144

TABLE III
ORGAN-WISE QUANTITATIVE EVALUATION COMPARED WITH TRADITIONAL U-NET

organ	$F1 - score$		AJI	
	U-Net	Proposed	U-Net	Proposed
breast	0.6291	0.8437	0.6204	0.6442
kidney	0.4557	0.8430	0.3951	0.6158
prostate	0.4087	0.8739	0.4556	0.5697
bladder	0.4064	0.8144	0.4915	0.5982
colon	0.3852	0.7280	0.3442	0.5566
lung	0.4998	0.7513	0.4282	0.6101
brain	0.6388	0.8435	0.4374	0.6767

w_{SRW} takes utilize of sufficient structural information in both Hematoxylin channel image and Eosin channel image. By calculating the likelihood of these two channels, the pixels which are weakly stained or contaminated can be highlighted. The effect of the predicted result of these pixels is emphasized during the training process so that our network could learn better features. The Boundary Enhancement Weight Map w_{BEW} gives high value for boundary pixels and potential touching region. Unlike other previous methods, we use detailed boundary annotations to construct a weight map instead of using a single morphological feature. We adopt MoNuSeg dataset for training and testing. Experiment results show the advantages of our proposed method in dealing with background noise and touching objects. This work is able to be seen as a parallel process with existing methods that focus on modifying the network structure. Our future work involves applying our weight maps to other network architecture, as well as further improving the loss function to avoid outliers caused by manually marked ground truth values.

REFERENCES

- [1] A.C.Ruifrok and D.A.Jhonston, "Quantification of histochemical staining by color deconvolution," *Analytical and quantitative cytology and histology* **23**, p. 291—299, August 2001.
- [2] A. Vahadane, T. Peng, A. Sethi, S. Albarqouni, L. Wang, M. Baust, K. Steiger, A. M. Schlitter, I. Esposito, and N. Navab, "Structure-preserving color normalization and sparse stain separation for histological images," *IEEE Transactions on Medical Imaging* **35**, pp. 1962–1971, Aug 2016.
- [3] J. Cheng and J. C. Rajapakse *, "Segmentation of clustered nuclei with shape markers and marking function," *IEEE Transactions on Biomedical Engineering* **56**, pp. 741–748, March 2009.
- [4] C. Jung and C. Kim, "Segmenting clustered nuclei using h-minima transform-based marker extraction and contour parameterization," *IEEE Transactions on Biomedical Engineering* **57**, pp. 2600–2604, Oct 2010.
- [5] S. Graham and N. M. Rajpoot, "Sams-net: Stain-aware multi-scale network for instance-based nuclei segmentation in histology images," in *2018 IEEE 15th International Symposium on Biomedical Imaging (ISBI 2018)*, pp. 590–594, April 2018.

- [6] F. A. Guerrero-Peña, P. D. Marrero Fernandez, T. Ing Ren, M. Yui, E. Rothenberg, and A. Cunha, "Multiclass weighted loss for instance segmentation of cluttered cells," in *2018 25th IEEE International Conference on Image Processing (ICIP)*, pp. 2451–2455, Oct 2018.
- [7] T. Falk, D. Mai, R. Bensch, Ö. Çiçek, A. Abdulkadir, Y. Marrakchi, A. Böhm, J. Deubner, Z. Jäckel, K. Seiwald, A. Dovzhenko, O. Tietz, C. D. Bosco, S. Walsh, D. Saltukoglu, T. L. Tay, M. Prinz, K. Palme, M. Simons, I. Diester, T. Brox, and O. Ronneberger, "U-net – deep learning for cell counting, detection, and morphometry," *Nature Methods* **16**, pp. 67–70, 2019.
- [8] N. Kumar, R. Verma, S. Sharma, S. Bhargava, A. Vahadane, and A. Sethi, "A dataset and a technique for generalized nuclear segmentation for computational pathology," *IEEE Transactions on Medical Imaging* **36**, pp. 1550–1560, July 2017.
- [9] Y. Zhou, O. F. Onder, Q. Dou, E. Tsougenis, H. Chen, and P. Heng, "Cia-net: Robust nuclei instance segmentation with contour-aware information aggregation," *CoRR* **abs/1903.05358**, 2019.
- [10] B. Chidester, T.-V. Ton, M.-T. Tran, J. Ma, and M. N. Do, "Enhanced rotation-equivariant u-net for nuclear segmentation," in *The IEEE Conference on Computer Vision and Pattern Recognition (CVPR) Workshops*, June 2019.
- [11] F. Mahmood, D. Borders, R. J. Chen, G. N. McKay, K. J. Salimian, A. S. Baras, and N. J. Durr, "Deep adversarial training for multi-organ nuclei segmentation in histopathology images," *CoRR* **abs/1810.00236**, 2018.
- [12] J. Xu, L. Xiang, G. Wang, S. Ganesan, M. Feldman, N. Shih, H. Gilmore, and A. Madabhushi, "Sparse non-negative matrix factorization (snmf) based color unmixingfor breast histopathological image analysis," *Computerized Medical Imaging and Graphics* **46**, 04 2015.
- [13] O. Ronneberger, P. Fischer, and T. Brox, "U-net: Convolutional networks for biomedical image segmentation," *CoRR* **abs/1505.04597**, 2015.
- [14] H. Kong, H. C. Akakin, and S. E. Sarma, "A generalized laplacian of gaussian filter for blob detection and its applications," *IEEE Transactions on Cybernetics* **43**, pp. 1719–1733, Dec 2013.
- [15] N. Kumar, R. Verma, D. Anand, Y. Zhou, O. F. Onder, E. Tsougenis, H. Chen, P. A. Heng, J. Li, Z. Hu, Y. Wang, N. A. Koohbanani, M. Jahanifar, N. Z. Tajeddin, A. Gooya, N. Rajpoot, X. Ren, S. Zhou, Q. Wang, D. Shen, C. K. Yang, C. H. Weng, W. H. Yu, C. Y. Yeh, S. Yang, S. Xu, P. H. Yeung, P. Sun, A. Mahbod, G. Schaefer, I. Ellinger, R. Ecker, O. Smedby, C. Wang, B. Chidester, T. V. Ton, M. Tran, J. Ma, M. N. Do, S. Graham, Q. D. Vu, J. T. Kwak, A. Gundu, R. Chunduri, C. Hu, X. Zhou, D. Lotfi, R. Safdari, A. Kascenas, A. O'Neil, D. Eschweiler, J. Stegmaier, Y. Cui, B. Yin, K. Chen, X. Tian, P. Gruening, E. Barth, E. Arbel, I. Remer, A. Ben-Dor, E. Siraztdinova, M. Kohl, S. Braunewell, Y. Li, X. Xie, L. Shen, J. Ma, K. D. Baksi, M. A. Khan, J. Choo, A. n. Colomer, V. Naranjo, L. Pei, K. M. Iftekharuddin, K. Roy, D. Bhattacharjee, A. Pedraza, M. G. Bueno, S. Devanathan, S. Radhakrishnan, P. Koduganty, Z. Wu, G. Cai, X. Liu, Y. Wang, and A. Sethi, "A multi-organ nucleus segmentation challenge," *IEEE Transactions on Medical Imaging* , pp. 1–1, 2019.
- [16] X. LIM, K. SUGIMOTO, and S. KAMATA, "Nuclei detection based on secant normal voting with skipping ranges in stained histopathological images," *IEICE Transactions on Information and Systems* **E101.D(2)**, pp. 523–530, 2018.
- [17] H. Chen, X. Qi, L. Yu, and P. Heng, "DCAN: deep contour-aware networks for accurate gland segmentation," *CoRR* **abs/1604.02677**, 2016.
- [18] H. A. Phoulady, D. B. Goldgof, L. O. Hall, and P. R. Mouton, "A framework for nucleus and overlapping cytoplasm segmentation in cervical cytology extended depth of field and volume images," *Computerized medical imaging and graphics : the official journal of the Computerized Medical Imaging Society* **59**, pp. 38–49, 2017.